J Mater Sci (2014) 49:8183–8191
DOI 10.1007/s10853-014-8527-2

Influence of deep cryogenic treatment on the thermal decomposition of Fe–C martensite

M. Preciado · M. Pellizzari

Received: 28 April 2014 / Accepted: 1 August 2014 / Published online: 4 September 2014

Abstract The beneficial effects of deep cryogenic treatment (DCT) at temperatures close to −180 °C on certain mechanical properties of steels are well known, although the metallurgical base mechanism of DCT still needs further clarification. In this study, the thermal decomposition of steel martensite (100Cr6) subjected to low-temperature soaking over different periods (SDCT = 5 min at −180 °C, LDCT = 24 h at −180 °C) is investigated by means of differential scanning calorimetry and dilatometry. The results were compared with those for the same conventionally quenched and tempered steel. Isochronal annealing experiments at different heating rates were performed, in order to highlight the main tempering stages and to obtain their relevant activation energies. DCT was clearly shown to lower the Ea of the pre-precipitation process more intensely than in the quenched steel. This result may probably be ascribed to an increased dislocation density and to the activation of the carbon segregation process in larger amounts of martensite. The precipitation of transition carbides was also enhanced by the low-temperature conditioning of martensite. As expected, DCT transformed the retained austenite, so that the corresponding peaks almost disappeared from both the dilatometric and the DSC patterns.

Electronic supplementary material The online version of this article (doi:10.1007/s10853-014-8527-2) contains supplementary material, which is available to authorized users.

M. Preciado (✉)
Department of Civil Engineering, University of Burgos, Avda. Cantabria s/n, 09006 Burgos, Spain
e-mail: mpreciado@ubu.es

M. Pellizzari
Department of Industrial Engineering, University of Trento, Via Sommarive 9, 38123 Trento, Italy
e-mail: Massimo.Pellizzari@ing.unitn.it

Introduction

Deep cryogenic treatment (DCT), consisting of soaking steel parts at low temperature, is claimed to be an effective way of improving the properties of industrial tools such as gears, shafts, rolls, and dies used in the manufacturing industry [1]. Many authors have referred to the benefits of controlled immersion in a cooling media [2–4]. Other mediums—brine, alcohol/water mixtures—were used before the advent of cryogenic processors, or cryoboxes, to enable controlled cooling and soaking in liquid nitrogen (LN). In accordance with the temperature, a distinction may be established between cold treatments (CT) at temperatures of around −80 °C and DCT at liquid nitrogen temperatures of around (−190 °C) [5, 6].

On a case-by-case basis, improvements in wear resistance, hardness and/or toughness were reported to occur immediately after a short soaking time or after prolonged (longer than 20 h) soaking [7]. In relation to wear resistance, cryogenic treatment of metals is said to be effective only in the presence of retained austenite after conventional treatment. In this case, the material benefits from the hardness increase were due to the austenite to martensite transformation [8]. On the other hand, a big increase in wear resistance was observed, even in the absence of retained austenite, and the finer distribution of carbides has been claimed to be the cause of this improvement [9].

According to the literature on cryo-treated steels, the improvement of mechanical properties can most probably be a consequence of the combined effect of retained

austenite to martensite transformation and the finer secondary carbides precipitation during tempering. However, some authors ascribe the main role to the conversion of retained austenite into martensite while others ones placed greater weight to the precipitation of fine carbides [10]. For tool steels [11], different reasons have been found as coarser cementite particles or delayed precipitation of alloying element carbides.

Research on the convenience of DCT prior to or after tempering has established that the mechanical properties are improved to a greater extent, when the cryogenic treatment is performed after quenching prior to tempering [12]. One of the reasons [13] is the occurrence of irreversible phase transformations cited above, which inhibits further transformation during cryogenic treatment. It has recently been demonstrated [14] that sub-zero treatment prior to tempering led to less increase in the volume fraction of secondary carbide particles and that the wear resistance ability of the studied steel was maximized by heat treatment procedure in the following order: austenitizing, quenching, DCT, and tempering.

Post-quench cooling at temperatures lower than Ms quite clearly permits martensitic transformations to continue in steels, provided that the retained austenite has not been excessively stabilized by prolonged exposure at room temperature. This transformation causes an increase in hardness accompanied by a general reduction in toughness. In secondary hardening steels, such as tool steels for hot and cold work and even high-speed steels, this transformation prompts a shift of the secondary hardness peak toward lower temperature [15, 16].

The idea of low-temperature conditioning of virgin martensite has been suggested [17] as the possible cause for very fine carbides distribution in steels. It consists of the formation of fresh martensite at low temperatures which is accompanied by the plastic deformation. During this plastic deformation, dislocation motion captures immobile carbon atoms and the carbon clusters that form can serve as sites for nucleation on fine η-carbide particles during subsequent tempering. Changes in the tetragonality of the martensite following cryogenic treatment have been studied as well as the way that this process might affect the carbides that are generated during tempering, depending on the number of defects in the lattice, martensite morphology, and type of alloying elements, among other factors [18]. Gavriljuk et al. [19] have also explained the reasons for the low tetragonality of fresh martensite, i.e., the capture of carbon atoms, by gliding dislocations in the course of the plastic deformation of martensite at low temperatures. Villa et al. [20] noted that temperature conditioning also results in the accommodation of transformation strain in martensite below a critical temperature (140 K for 100Cr6 steel), generating additional nucleation sites for the precipitation of transition carbides during tempering. In the same reference, it is also stated that during the austenite to martensite transformation at low temperature (above 140 K), compressive strains built up in austenite and were found to be retained also after tempering. In a second study [21], the same authors proved that cryogenic treatment had no effect on the tetragonality of martensite and it was concluded that enhanced precipitation of transition carbides was only possible for long isothermal holding at cryogenic temperatures.

Further studies [22–25] evidenced that cryogenic treatment can facilitate the formation of carbon clustering, increase carbide density during tempering, and obtain a more homogeneous carbide distribution, thereby improving the wear resistance of steels.

Then, the influence of DCT on the decomposition of martensite under tempering appears clear as this kind of treatment affects the processes involved in the stages of tempering that could be identified as follows [26]:

Stage I–II: "pre-precipitation processes"; these stages occur below 80 °C and involve carbon enrichments (I) and the periodic arrangement of enrichments (II).
Stage III: precipitation of transition ε/η carbides; this stage occurs between 80 and 180 °C.
Stage IV: transformation of retained austenite (γ) into ferrite (α) and cementite (θ), between 200 °C and 350 °C (in [20] it was observed that the retained austenite decomposed at lower temperatures compared to conventionally quenched samples); this stage occurs in two successive steps
Step 1: $\gamma \rightarrow \alpha + \gamma_{\uparrow\% \text{ C}}$ (expansion)
Step 2: $\gamma_{\uparrow\% \text{ C}} \rightarrow \alpha + \theta$ (contraction)
Stage V: conversion of transition carbides into cementite; this stage occurs between 250 and 500 °C.

Mittemeijer and other authors conducted extensive studies on the tempering behavior of carbon and carbon–nitrogen martensite, using differential scanning calorimetry DSC, dilatometry, and XRD analysis [20, 26–29]. The different tempering stages can be clearly separated and identified, particularly using nonisothermal annealing. The proposed transformation mechanism is more complicated in alloyed steels subjected to DCT (tool and high-speed steels are typically subjected to DCT) because Cr, Mo, W, and V complicate the thermal decomposition of martensite and retained austenite during tempering: all transformation stages are shifted to higher temperature, and precipitation of complex alloy carbides is added (superimposed) to those of cementite and iron transition carbides [30, 31].

In this study, the thermal decomposition of as-quenched 100Cr6 bearing steel subjected to different DCTs is analyzed. The influence of low temperature soaking (−196 °C for 5 min and 24 h) on the tempering behavior is studied.

Samples were rapidly cooled by immersion in LN immediately after quenching, i.e., under conditions far from current processing practice. According to previous statement, this would reduce as much as possible any isothermal decomposition of retained austenite. Similarly, the relatively high heating rate to room temperature suppresses any cluster formation and moves this pre-precipitation stage of transformation during tempering, studied by differential scanning calorimetry and dilatometry. A systematic attempt was made to reduce the influence of secondary factors (sample dimension, time interval between quenching and tempering/DCT…), in order to obtain accurate values.

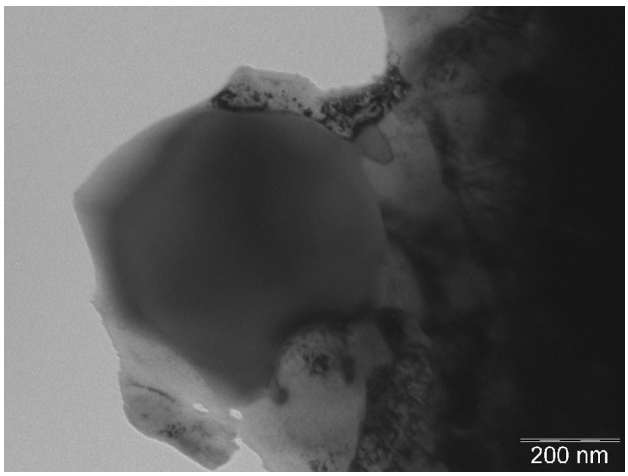

Fig. 1 TEM image of undissolved cementite

Materials and methods

The 100Cr6 bearing steel used in this study contained 1.0 % C and 1.5 % Cr and minor alloying additions. It was delivered in rounds of 4 mm diameter. Cylindrical samples of 10 mm length were obtained for dilatometric measurements, carried out using a Bähr dilatometer model 805A. Each single sample was vacuum (10^{-4} mbar) austenitized at 840 °C for 15 min and quenched in pressurized nitrogen atmosphere allowing a cooling rate of 25 °C s^{-1}, i.e., high enough to obtain a full martensite microstructure. Two DCTs were evaluated: a short one (SDCT), comprising direct immersion of the steel in the liquid nitrogen and a total soaking time of 5 min; and a long one (LDCT), with a soaking time of 24 h. A simple as-quench sample (Q) was used for comparing the results.

Dilatometry was performed immediately after quenching and DCT, by heating the sample up to 500 °C at heating rates of 5, 10, 15, and 20 °C min^{-1}. As described in [22], the data were mathematically averaged over time and subsequently differentiated by temperature, in order to define the different transformation peaks during tempering. The activation energy was obtained for the precipitation of η/ε transition carbides, the decomposition of retained austenite, and the precipitation of cementite.

Differential scanning calorimetry was performed with a Perkin Elmer DSC7 calorimeter in a protective atmosphere of argon. The disk specimen (60 and 90 mg mass) was cut from the cylindrical sample immediately after DCT. After weighing, the sample was heated from 30 to 500 °C at a heating rate of 5, 10, 15, and 20 °C min^{-1}. Pure aluminum disks were used as the reference material. The baseline was determined by carrying out a second scan at the same heating rate. It was possible to determine the activation energy at all tempering stages.

Both the dilatometric and the DSC tests were very rigorously time-scheduled, allowing no intermediate transformations (room tempering) between quenching and the DCTs. The time between DCT and the preparation of samples for the DSC tests was also minimal. The amount of retained austenite was determined by means of XRD analysis using Mo K-alpha radiation.

The Kissinger-like method was used to obtain the activation energy for the phase transformation occurring during tempering, according to Eq. (1) [27].

$$\frac{\ln\left(T_{f'}^2\right)}{\phi} = \frac{E}{RT_{f'}} + \text{constant}, \tag{1}$$

where R is the gas constant, $T_{f'}$ is the transformation temperature corresponding to a certain fraction (f') of the transformed phase, and ϕ is the heating rate in °C min^{-1}. When ln $((T_{f'}{}^2)/\phi)$ is plotted as a function of $1/T_{f'}$, the slope of the straight line indicates a value for activation energy. The correlation coefficient R was higher than 0.9 in all cases; a high confidence level that adds to the reliability of the results.

Results

The microstructure of the as-quenched steel consisted of a primary martensite matrix and a small fraction of finely dispersed undissolved cementite showing submicrometric size (Fig. 1), which could not be determined by quantitative metallographic techniques. The fine size of precipitates did not allow their identification even by XRD analysis (Fig. 2). By thermodynamic calculations carried out by Thermo-Calc software, the amount of carbide has been estimated close to 4.5 % vol. The calculated carbon content in the parent austenite was 0.8 wt%, corresponding to an Ms of 191 °C obtained by dilatometry. The post-quenching amount of retained austenite (r.a.), determined by X-ray

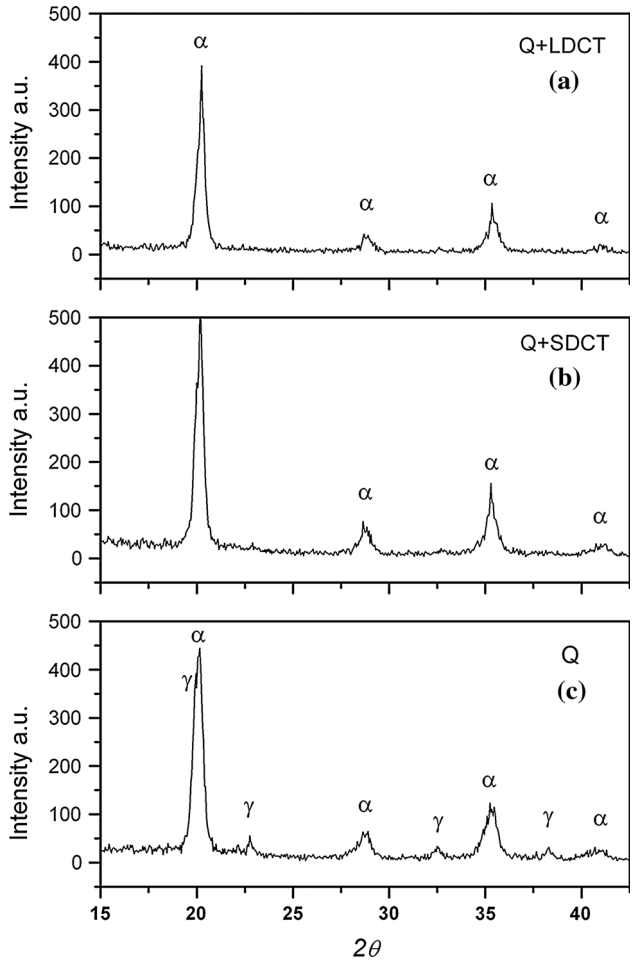

Fig. 2 X-Ray diffraction patterns for **a** Long Q + LDCT, **b** Short Q + SDCT, and **c** Q, as-quenched

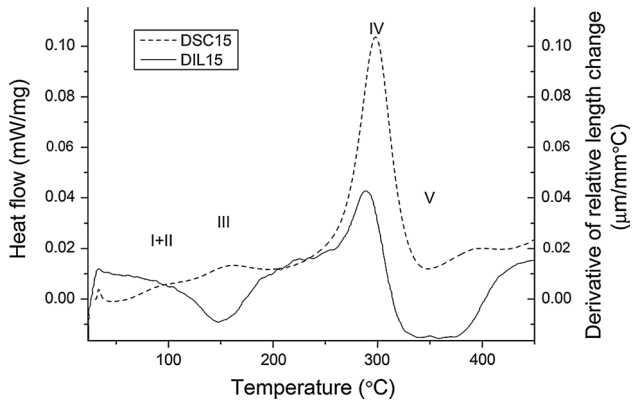

Fig. 3 DSC *curve* and derivative of relative length change *curve* of as-quenched steel during isochronal annealing at a heating rate of 15 °C min^{-1}

diffraction was about 7 % (Fig. 2a), is relatively low due to the low austenitizing temperature used to quench the samples. A small well-defined austenite reflection (22°) was still present after the SDCT (Fig. 2b), while no more traces were detected in LDCT (Fig. 2c), suggesting that the austenite content fell below the threshold detection limit of XRD (2 %).

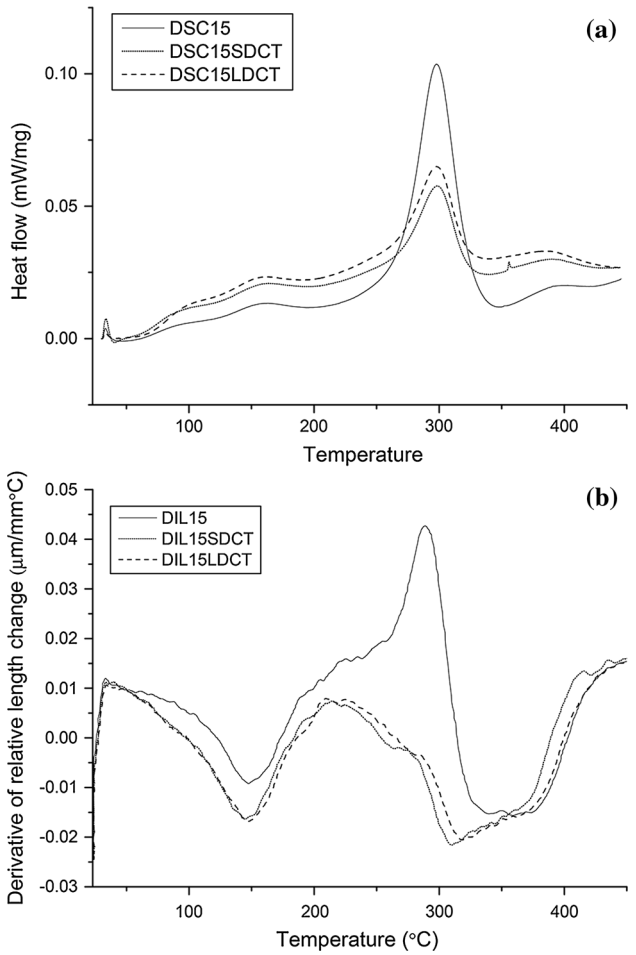

Fig. 4 **a** DSC *curve* and **b** derivative of relative length change, of steel after Q (Quenching), Q + SDCT, and Q + LDCT during isochronal annealing at a heating rate of 15 °C min^{-1}

Figure 3 shows the typical aspect of DSC (dashed line) and dilatometric curves (continuous line) recorded for the as-quenched steel. A good correspondence in the temperatures between the peaks in DSC and dilatometry is evidenced. The DSC curve represents the heat evolution of the sample subjected to tempering. When a change that involves a significant heat release occurs, a peak appears in the DSC curve. These peaks are associated to the different tempering stages. The dilatometric curve reflects the changes in specific length, and the peaks in the derivative of the relative length change allow the stages of tempering to be identified.

Figure 4 displays the DSC curves (Fig. 4a) and the derivative of the relative length change (Fig. 4b) of the samples after quenching and different DCTs on isochronal annealing at 15 °C min^{-1}. Similar results were also

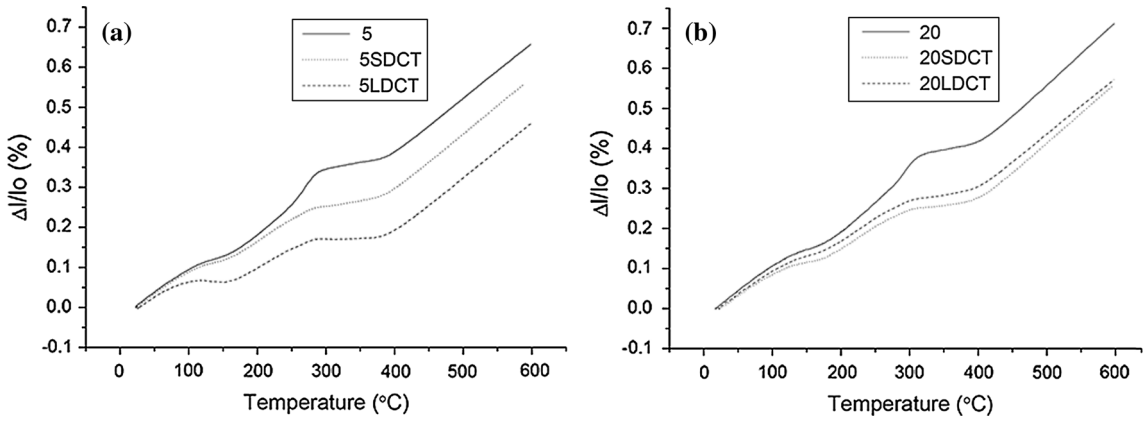

Fig. 5 Percentage of length change at **a** 5 °C min^{-1}, **b** 20 °C min^{-1}

Table 1 Identification of the transformations occurring during the tempering of the as-quenched martensite (Q), further subjected to short (Q + SDCT)and long (Q + LDCT) deep cryogenic treatment

	DSC Q	DSC Q + SDCT	DSC Q + LDCT	DIL Q	DIL Q + SDCT	DIL Q + LDCT
STAGE I and II						
I Carbon enrichments	89 °C	90 °C	95 °C			
II Periodic arrangement of enrichments	77.8 KJ mol^{-1}	62.3 KJ mol^{-1}	54.8 K mol^{-1}			
(25–100 °C)						
STAGE III						
ε/η Precipitation	151 °C	152 °C	152 °C	147 °C	144 °C	141 °C
(80–180 °C)	92.2 K mol^{-1}	92.7 KJ mol^{-1}	89.1 KJ mol^{-1}	98.8 KJ mol^{-1}	91.8 KJ mol^{-1}	93.1 KJ mol^{-1}
STAGE IV						
$\gamma \rightarrow \alpha + \theta$	290 °C	291 °C	291 °C	281 °C	–	_
(200–350 °C)	114.8 KJ mol^{-1}	125.8 KJ mol^{-1}	124.7 KJ mol^{-1}	134.4 KJ mol^{-1}	_	–
STAGE V						
$\xi/\eta \rightarrow \alpha + \theta$	382 °C	385 °C	382 °C	347 °C	_	_
(250–500 °C)	_	281.8 KJ mol^{-1}	235.9 KJ mol^{-1}	185.3 KJ mol^{-1}	_	_

obtained at 5, 10, and 20 °C min^{-1}. The stages I + II are only evident in the DSC curves (there is no length change involvement). The stage IV corresponding to the decomposition of the retained austenite is clearly represented for the as-quench sample in both techniques but for the samples submitted to DCT, the peak associated to this stage appears only in the DSC curves. In the dilatometric curves, the stage V overlaps with the second step of the stage IV (both imply contraction) but in the DSC curves a soft peak could be identified at this stage.

Figure 5 shows the percentage length change of two isochronal annealing treatments, obtained by dilatometry. The linear expansion coefficient of the Q sample is higher than the coefficient of the cryogenic-treated samples. This is due to the higher amount of retained austenite.

Table 1 resumes the activation energy values obtained by differential calorimetry (DSC) and dilatometry (DIL). As expected, the transformation peak temperatures slightly rise by increasing the heating rate, ϕ, and the temperature that appears in the table corresponds to the mean temperature recorded for the different rates. An empty box means that the stage was not detected by the considered technique with the exception of the energy of activation corresponding to the stage V by DSC in which the result was not reliable, i.e., the Adj. R-square of the energy of activation calculated was less than 0.98.

The activation energies at different sources are summarized in Table 2, although it has to be taken into account that the steels used by different authors were not of identical composition.

Table 2 Data of activation energies found in the literature

Stage I				
Clustering	$E = 79$ kJ mol^{-1} [26]	$E = 81$–94 kJ mol^{-1} [29]	$E = 81$ kJ mol^{-1} [33]	Diffusion of carbon in martensite: 67–70 kJ mol^{-1} [34]
Stage II				
Segregation of carbon atoms to lattice defects	$E = 83$ kJ mol^{-1} [26]			
Stage III				
ε/η Precipitation	$E = 126$ kJ mol^{-1} dilatometric study [26] $E = 111$ kJ mol^{-1} DSC study [26]	$E = 103$–120 kJ mol^{-1} [32]	$E = 93.52$ kJ mol^{-1} [36]	Pipe diffusion on iron: 134 kJ mol^{-1} [32]
Stage IV				
γ Decomposition	$E = 132$ kJ mol^{-1} [26]	$E = 135$–156 kJ mol^{-1} [29]		Diffusion of C in γ-Fe: 128 kJ mol^{-1} [38]
Stage V				
Transformation of carbides	$E = 203$ kJ mol^{-1} [26]	$E = 163$–212 kJ mol^{-1} [29]		Volume diffusion of iron: 251 kJ mol^{-1} [33]

Discussion

I–II. Pre-precipitation processes

The heat evolution produced due to pre-precipitation processes can be detected below 100 °C. Because of the low-length change pertaining to these transformations, pre-precipitation processes are not evidenced by dilatometry (Fig. 4b) [29]. On the other hand, their exothermic contribution is relatively more intense so that they are clearly highlighted by calorimetric signal (Fig. 4a). It is believed that this is enhanced by the processing conditions used in this work, particularly the high heating rate to room temperature that suppresses (hinders) possible clustering, moving it during the first stages of tempering.

The heat effect due to carbon enrichment (I) and the periodic arrangement of enrichments (II) are both intensified after soaking in liquid nitrogen than after conventional quenching of the samples, as confirmed by the stronger heat release of SDCT and LDCT samples.

Examining the DSC curves in Fig. 4a, no marked difference is observed when comparing the samples kept for short (SDCT) or long (LDCT) periods at low temperature, even though a slightly higher heat release was shown after LDCT. There were no significant changes in the temperature ranges between cryogenically treated and untreated steel (Table 1).

The activation energy calculated for the quenched steel (77.8 kJ mol^{-1}) is in good agreement with the values reported in the literature (Table 2) and is compatible with the migration of interstitially dissolved atoms to dislocations in α' martensite [34].

Although neither carbon atom clustering nor the segregation of carbon atoms in lattice defects involves large-scale changes, it was the atom clustering process that led to a minimum change in specific volumes, as the carbon atoms remained dissolved in the iron matrix; hence, the average lattice parameter and the volume remained unaffected [14]. The absence of peaks in the dilatometric signal supports clustering to be the dominant effect. In this sense, activation energies of SDCT and LDCT (62.5 and 54.8 kJ mol^{-1}, respectively) lower than that of the *Q* sample (77.8 kJ mol^{-1}) evidence an apparent activation due to the cryogenic treatment. These values provide numerical evidence of the effect that DCT has on the tempered martensite meaning a faster redistribution of interstials toward lattice defects. According to previous findings, this is promoted by the formation of martensite at cryogenic temperatures which conditions existing martensite [20, 35]. A plausible explanation is the higher quantity of dislocations introduced by DCT, which represent preferential sites for the segregation of carbon or the capture of carbon atoms following the generation of dislocations and dislocation glide during the plastic deformation of the virgin martensite, as it forms at low temperatures [17].

III. Precipitation of transition carbides

The precipitation of transition carbides occurred at around 150 °C and was associated with a pronounced heat release (Fig. 4a) and length decrease (Fig. 4b) [29].

From dilatometric curves, where overlapping with pre-precipitation processes is absent, an improved precipitation of ε/η carbides is evidenced after DCT. Indeed, the activation energy values calculated for the as-quenched and cryogenically treated samples do not show significant differences, meaning that the mechanism does not change. It is likely that the stronger precipitation may be simply ascribed to the higher fraction of martensite after DCT.

In general, the values of the activation energy for the tested specimens were lower than those previously proposed by other authors for different steels. A calculated value depending on the quantity of carbon and chromium is given by the following formula [36]

$$E = 75.4 + 35.6 * \mathrm{wt}(\%)\mathrm{C} - 11.1 * \mathrm{wt}(\%)\mathrm{Cr}\ \mathrm{KJ/mol}. \quad (2)$$

So, the activation energy increases with an increase in the carbon content of the martensite and decreases with an increase in chromium content. This pattern is explained by King and Glover [37] in terms of the tetragonality of the martensite, which increases the value of the activation energy because this last one is mainly associated with the energy barrier opposing the passage of the carbon atoms through the prohibited octahedral sites. The chromium is a carbide-forming element; then, it is supposed to reduce the thermodynamic activity coefficient of the dissolved carbon. Applying the formulae to present steel, a value of activation energy of 94.9 kJ mol^{-1} is obtained, confirming a very good agreement with the experimental values (Table 1). This activation energy lies between that for diffusion of C in α-Fe and that for diffusion of iron along dislocations.

IV. Transformation of retained austenite

The decomposition of retained austenite into ferrite and cementite causes a high heat evolution and a net length increase (Fig. 4). An exothermic peak is observed in the temperature range between 250 and 350 °C. The peak intensity is lower for SDCT and LDCT, due to the preliminary cryogenic transformation of austenite. However, the decomposition of this phase starts before the DSC peak. In [33], X-ray diffraction measurements demonstrated that a decrease in the $\{200\}_\gamma$ peak intensity, associated with an increase of the lattice parameter, started at 150 °C (for FeC steel), i.e., much before the main calorimetric peak at 270 °C. Similarly, for present steel in the as-quenched state, the expansion associated to the formation of a C-enriched austenite and ferrite (Step 1) starts at about 220 °C, while the peak is located at around 290 °C.

The simultaneous precipitation of cementite from austenite (length decrease) overlaps the expansion of the previous step, as shown by dilatometry (Fig. 5) and spreads over a wider temperature range compared to the pure iron/carbon systems. A similar behavior was also reported by Morra for the same steel [29]. It can be observed that the DSC peaks did not disappear after DCT, which was proved to provide the almost complete transformation of this phase. Correspondingly, only a slight length increase in the dilatometric curves of cryo-treated samples is present.

The activation energy value obtained by DSC for the decomposition of retained austenite in the as-quenched specimens was around 114.8 kJ mol^{-1} and slightly higher values (approximately 125 kJ mol^{-1}) were observed for SDCT and LDCT in agreement with the activation energy value for the diffusion of C in γ-Fe 129 kJ mol^{-1}, obtained by graphical interpolation from Fig. 9 in Reference 38 in which it is shown how the energy of activation decreases, when the percentage of carbon increases.

In the case of dilatometry, the peak can be regarded as an average apparent value of two transformation steps (expansion and contraction). The value of 134.4 kJ mol^{-1} was obtained for a peak temperature of 281 °C (average temperature of 191 °C for DSC).

The difference between peak temperatures and the change of instrument to obtain the results can explain the discrepancy of activation energy values for Q (Table 1) by DSC and dilatometry and supports that any reasonable comparison between Q and SDCT/LDCT is possible considering DSC only. In this sense, the decomposition of austenite in SDCT and LDCT samples showed higher activation energy than in the as-quenched steel. The compression generated in austenite during DCT [20] could be the reason for its higher stability.

V. Precipitation of cementite

The phase transformation, highlighted by a discrete heat release between 350 and 450 °C (Fig. 4a), is associated with the precipitation of cementite from ε/η carbides, carbon segregated in dislocations and carbon in solid solution within martensite [39]. It is likely that this last contribution will account for a minor extent only, since the degree of martensite tetragonality was shown to reach unit value at temperature much lower than that for the precipitation of cementite [40]. The process is accompanied by a large length decrease, occurring after the precipitation of cementite from austenite decomposition, and exhibits a strong overlap with this latter process (Fig. 4b).

The activation energy values, respectively, 235.9 and 281.8 kJ mol^{-1}, could only be accurately measured in the SDCT and LDCT samples. These values are similar to the activation energy value of 251 kJ mol^{-1} for the volume diffusion of iron. The peaks are at a temperature of about 385 °C. The value obtained by dilatometry for the Q sample is much lower (185.3 kJ mol^{-1}). According to literature data, the effective activation energy lies between the value of pipe diffusion of iron (134 kJ mol^{-1}) and the value of volume diffusion of iron (251 kJ mol^{-1}). Finally, the calculated activation energies suggest a slower precipitation in deep cryogenically treated steel. This is rather curious, in view of the faster precipitation kinetics of transition carbides after low temperature soaking seems to

confirm a higher thermal stability of these particles compared to the quenched steel. Nevertheless, this result would need further investigations.

Conclusions

The tempering behavior of 100Cr6 bearing steel was studied in the as-quenched state and after further DCT by direct immersion in liquid nitrogen for a short (5 min, SDCT) and long (24 h, LDCT) soaking time. Differential scanning calorimetry and dilatometry were employed.

Pre-precipitation stage, involving carbon enrichments and the periodic arrangement of enrichments (clustering), is enhanced by DCT and the lower activation energy highlighted a faster redistribution of C. The activation energy decreased when increasing DCT holding time. According to the available literature, this evidence could be ascribed to the conditioning of martensite at cryogenic temperature, i.e., the introduction of a high density of dislocations which are preferential sites for segregation and clustering.

An enhanced carbide precipitation has been evidenced after DCT, while the activation energy measured was similar to that of the as-quenched steel.

Retained austenite was almost completely eliminated by SDCT. A longer soaking at cryogenic temperature (LDCT) caused further transformation, supporting the formation of thermally activated martensite. The decomposition of austenite in SDCT and LDCT samples showed higher activation energy than in the as-quenched steel, compatible with its higher stability due to compressive stresses.

References

1. Brown J (1995) Big chill to extend gear life. Power Transm Des pp 59–61
2. Zhirafar S, Rezaeian A, Pugh M (2007) Effect of cryogenic treatment on the mechanical properties of 4340 steel. J Process Technol 186(1–3):298–303
3. Babu PS, Rajendran P, Rao KN (2005) Cryogenic treatment of M1, En19 and H13 tool steels to improve wear resistance. J Inst Eng India MM 86:64–67
4. Gulyaev AP (1998) Cold treatment of steel. Mat Sci Heat Treat 40(11):449–455
5. Carlson EA (1991) Cold treating and cryogenic treatment of steel, ASM Handbook 4. ASM International, Metals Park, pp 203–206
6. Collins DN (1996) Deep cryogenic treatment of tool steels: a review. Heat Treat Met 23:40–42
7. Das D, Dutta AK, Ray KK (2009) Influence of varied cryo-treatment on the wear behaviour of AISI D2 steel. Wear 266(1–2):297–309
8. Barron RF (1982) Cryogenic treatment of metals to improve wear resistance. Cryogenics 8:409–413
9. Meng F, Tagashira K, Sohma H (1994) Wear resistance and microstructure of cryogenic treated Fe-1.4Cr-1C bearing steel. Scr Metall Mater 31(7):865–868
10. Gill S, Singh J, Singh R, Singh H (2011) Metallurgical principles of cryogenically treated tool steels –a review on the current state of science. Int J Adv Manuf Technol 54:59–82
11. Gavriljuk VG, Sirosh VA, Petrov YUN, Tyshchenko AI, Theisen W, Kortmann A (2014) Carbide precipitation during tempering of a tool steel subjected to deep cryogenic treatment. Metall Mater Trans A 45A:2453–2465
12. Dong Y, Xiaoping L, Hongshen X (1998) Deep cryogenic treatment of high-speed steel and its mechanism. Heat Treat Met 3:55–59
13. Lal DM, Renganarayanan S, Kalanidhi A (2001) Cryogenic treatment of argument wear resistance of tool and die steels. Cryogenics 41(3):149–155
14. Yan XG, Li DY (2013) Effects of the sub-zero treatment condition on microstructure, mechanical behaviour and wear resistance of W9Mo3Cr4 V high speed steel. Wear 302:854–862
15. Pellizzari M, Molinari A, Girardini L, Maldarelli L (2008) Deep cryogenic treatment of AISI M2 high speed steel. Int J Microstruct Mat 3(2–3):383–390
16. Pellizzari M (2008) Influence of deep cryogenic treatment on the properties of conventional and PM high speed steels. Metall Ital 9:7–22
17. Tyshchenko AI, Theisen W, Oppenkowski A (2010) Low-temperature martensitic transformation and deep cryogenic treatment of a tool steel. Mater Sci and Eng A 527:7027–7039
18. Wierszyllowski I, Samolczyk J, Wieczorek S, Adrzejewska E, Marcinkowska A (2008) The influence of deep cryogenic treatment on transformation during tempering of quenched D2 steel Studies of XRD structures, DSC, dilatometry hardness and impact energy. Defect Diffus Forum 273–276:731–739
19. Gavriljuk VG, Theisen W, Sirosh VV (2013) Low-temperature martensitic transformation in tool steels in relation to their deep cryogenic treatment. Acta Mater 61:1705–1715
20. Villa M, Pantleon K, Somers MAJ (2014) Evolution of compressive strains in retained austenite during sub-zero Celsius martensite formation and tempering. Acta Mater 65:383–392
21. Villa M, Pantleon K, Somers MAJ (2013) Enhanced carbide precipitation during tempering of sub-zero celsius treated AISI 52100 bearing steel. In: Proceedings of the heat & surface engineering conference and expo, Chennai
22. Huang JY, Zhu YT, Liao XZ, Beyerlein IJ, Bourke MA, Mitchell TE (2003) Microstructure of cryogenic treated M2 tool steel. Mater Sci and Eng A A339:241–244
23. Akhbarizadeh A, Shafyei A, Golozar MA (2009) Effects of cryogenic treatment on wear behaviour of D6 tool steel. Mater Des 30:3259–3264
24. Yen PL (1997) Formation of fine eta Carbides in special cryogenic and tempering process key lo improved properties of alloy steels. Ind Heat l.1:40–44
25. Kelkar R, Nash P, Zhu Y (2003) The mechanism of property enhancement in M2 tool steel by cryogenic treatment. In: 45th MWSP Conference Proceedings pp 13–19
26. Cheng L, Brakman CM, Korevaar BM, Mittemeijer EJ (1988) Stages in tempering of a martensitic 1.13 per cent carbon steel. Met Trans A 19A:2415–2426
27. Mittermeijer E (1992) Analysis of the kinetics of phase transformations. J Mater Sci 27:3977–3987. doi:10.1007/BF01105093
28. Haseeb ASMA, Arita M, Hayasi Y (2001) Thermal decomposition study of electrodeposited Fe-C and Fe-Ni-C alloys by differential scanning calorimetry. J Mat Sci 36:4739–4743. doi:10.1023/A:1017931106376
29. Morra PV, Bottger AJ, Mittemeijer EJ (2001) Decomposition of iron based martensite. A kinetic analysis by means of differential

scanning calorimetry and dilatometry. J Therm Anal Cal 64:905–914
30. Pellizzari M, Molinari A, Gialanella S, Straffelini G (2001) Effetto del trattamento criogenico sulle proprietà microstrutturali dell'acciaio AISI H13. Metallurgia Italiana 1(1):21–27. doi:10.1023/A:1017931106376
31. Pellizzari M, Molinari A (2002) A deep cryogenic treatment of cold work tool steel. In: Proceedings of 6th International Tooling Conference, pp 547–557
32. Cohen M (1970) Self-diffusion during plastic deformation. Inst Met Trans J I M 11:145–151
33. Van Genderen MJ, Isac M, Bottger A, Mitemeijer EJ (1997) Aging and tempering behaviour of Iron-Nickel-Carbon and Iron-Carbon Martensite. Metall Trans A 28A:545–561
34. Lee SH, Lee JC, Choi JY, Nam WJ (2010) Effects of deformation strain and ageing temperature on strain aging behaviour in a 304 stainless steel. Met Mater Int 16:21–26
35. Villa M, Hansen MF, Pantleon K, Somers MAJ, (2013) In situ investigation of martensite formation in AISI 52100 bearing steel at subzero Celsius temperature. In: Proceedings of 2nd Mediterranean Conference & new Challenges on heat treatment and surface engineering, Dubrovnik, pp 237–244
36. Wierszgyllowski I, Jakubowski J (1986) The influence of transformation progress on the activation energy changes during low temperature tempering of quenched steel. Scri Metall 20:49–54
37. King HW, Glover SG (1906) Influence of alloying elements on the first stage of tempering in high-carbon steels. J Iron Steel Inst 193:281–288
38. Batz W, Mehl RF (1950) Diffusion coefficient of carbon in austenite. Trans AIME 188:553–560
39. Han K, Van Genderen MJ, Bottger A, Zandbergen HW, Mittemeijer EJ (2001) Initial stages of Fe-C martensite decomposition. Phil Mag A 81(3):741–757
40. Perez M, Sidoroff C, Vincent A, Esnouf C (2009) Microstructural evolution of martensitic 100Cr6 bearing steel during tempering: from thermoelectric power measurements to the prediction of dimensional changes. Acta Mater 57:3170–3181